Determination of a complete set of coupling constants in ^{13}C-labeled oligonucleotides

H. Schwalbe[a], J.P. Marino[b], G.C. King[c], R. Wechselberger[a], W. Bermel[d] and
C. Griesinger[a],*

[a]*Institut für Organische Chemie, Universität Frankfurt, Marie-Curie-Strasse 11, D-60439 Frankfurt, Germany*
[b]*Department of Chemistry, Yale University, 225 Prospect Street, New Haven, CT 06511, U.S.A.*
[c]*Department of Biochemistry and Cell Biology, Rice University, Houston, TX 77204, U.S.A. and School of Biochemistry and Molecular Genetics, University of New South Wales, P.O. Box 1, Kensington, Australia 2033*
[d]*Bruker Analytische Messtechnik GmbH, Silberstreifen, D-76287 Rheinstetten, Germany*

SUMMARY

Three experiments are introduced to determine a complete set of coupling constants in RNA oligomers. In the HCCH-E.COSY experiment, the vicinal proton–proton coupling constants can be measured with high accuracy. In the P-FIDS-CT-HSQC experiment, vicinal proton–phosphorus and carbon–phosphorus couplings are measured that depend on the phosphodiester backbone torsion angles β and ε. In the refocussed HMBC experiment, vicinal carbon–proton couplings are measured that depend on the glycosidic torsion angle χ.

INTRODUCTION

Homo- and heteronuclear coupling constants offer a wealth of information for use in NMR structure determination. For oligonucleotides, homonuclear ^{3}J(H,H) couplings provide insight into sugar ring conformation (van Wijk et al., 1992), while ^{3}J(H,P) and ^{3}J(C,P) couplings yield information about the phosphodiester backbone conformation. In favourable instances, the conformation of the glycosidic bond (syn versus anti) can be determined from vicinal couplings of H1' to the carbon atoms in the nucleobase (Lamieux et al., 1978). Althought the importance of coupling constant data for oligonucleotide conformation analysis has long been recognized and has recently received increased attention (Varani and Tinoco, 1991), methods for their precise determination in oligonucleotides are not well developed for various reasons. Here we introduce
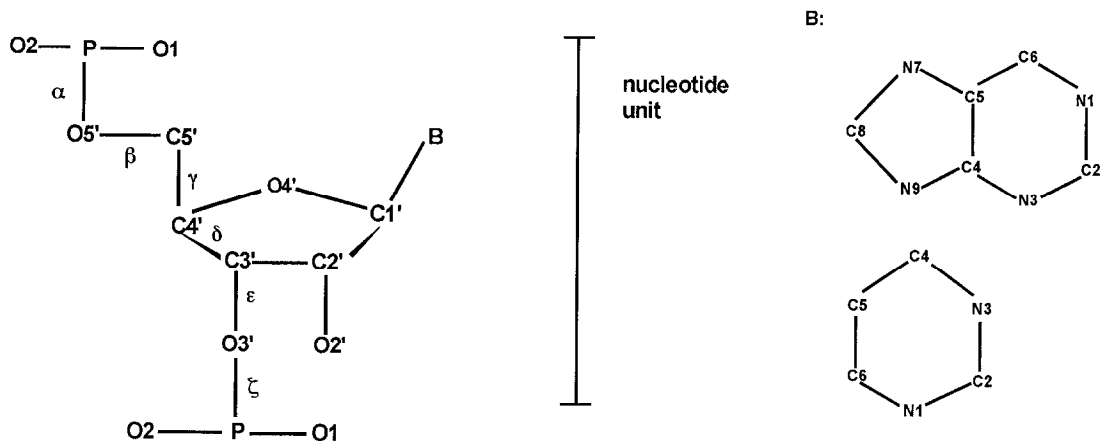
---

*To whom correspondence should be addressed.

632

Fig. 1. Definition of the constitutional and conformational parameters for oligonucleotides. Torsion angles: $\alpha = O3'_{(n-1)}$-P-O5'-C5'; $\beta = $ P-O5'-C5'-C4'; $\gamma = $ O5'-C5'-C4'-C3'; $\delta = $ C5'-C4'-C3'-O3'; $\varepsilon = $ C4'-C3'-O3'-P$_{(n+1)}$; $\zeta = $ C3'-O3'-P$_{(n+1)}$-O5'$_{(n+1)}$; $\nu_0 = $ C4'-O4'-C1'-C2'; $\nu_1 = $ O4'-C1'-C2'-C3'; $\nu_2 = $ C1'-C2'-C3'-C4'; $\nu_3 = $ C2'-C3'-C4'-O4'; $\nu_4 = $ C3'-C4'-O4'-C1'; χ(pyrimidines) = O4'-C1'-N1-C2; χ (purines) = O4'-C1'-N9-C4.

methods for the determination of a complete set of coupling constants in RNA oligomers, which depend on the backbone as well as on the sugar ring conformation. The methods partly rely on the use of uniformly ^{13}C-labeled oligonucleotides, which have recently become available (Batey et al., 1992; Nikonowicz et al., 1992; Nikonowicz and Pardi, 1992; Michnicka et al., 1993). The nomenclature and experimentally accessible coupling constants used to determine the torsion angles in RNA and DNA oligomers (Sänger, 1988) are listed in Fig. 1 and in Table 1.

HOMONUCLEAR [3]J(H,H) COUPLING CONSTANTS

Vicinal proton–proton couplings can be measured in homonuclear experiments with the P.E.COSY experiment (Griesinger et al., 1985, 1986, 1987; Müller, 1987; Marion and Bax, 1988). In RNA, however, this method is only applicable for the measurement of the H4' to H5' and H5" coupling constants, since three mutually coupled spins are required. The other proton–proton coupling constants in the ribose ring cannot be determined with this method.

For ^{13}C-labeled sugar moieties, all [3]J(H,H) coupling constants can be obtained from the HCCH-E.COSY experiment (Griesinger and Eggenberger, 1992), the feasibility of which has been demonstrated for the measurement of [3]J(H$^\alpha$,H$^\beta$) couplings in proteins (Eggenberger et al., 1992). The pulse sequence used for ribonucleotides is shown in Fig. 2A. The experiment can run in either 2D or 3D formats. In the 2D version, for example, C1' is correlated with H2'. The schematic multiplet pattern is shown in Fig. 3A. The [1]J(C1',H1') coupling constant is used as associated coupling in the C1',H2' cross peak to resolve the [3]J(H1',H2') coupling. For the determination of the homonuclear coupling constants in HC(i)C(i ± 1)H$_n$ fragments (n = 1,2,3), the C(i),H(i ± 1) cross peaks can be interpreted directly. Methods for the determination of the coupling constants from the H$_2$C(i)C(i ± 1)H$_n$ cross peaks (n = 1,2,3) (i.e., starting in ω_1 from methylene moieties) have been discussed by Griesinger and Eggenberger (1992). For the investigation of larger RNA fragments along these lines, 3D experiments are necessary to achieve sufficient

TABLE 1
COUPLING CONSTANTS USED TO DETERMINE THE TORSION ANGLES IN RNA AND DNA OLIGOMERS

Torsion angle	Coupling constant	Experiment
α		
β	$^3J(H5',P)$; $^3J(H5'',P)$; $^1J(C4',P)$	P-FIDS-HSQC
γ	$^3J(H4',H5')$; $^3J(H4',H5'')$	HCCH-E.COSY
$\delta = v_3 + 180°$	$^3J(H3',H4')$	HCCH-E.COSY
ε	$^3J(H3',P)$; $^3J(C4',P)$; $^3J(C2',P)$	P-FIDS-HSQC
ζ		
v_0		
v_1	$^3J(H1',H2')$	HCCH-E.COSY
v_2	$^3J(H2',H3')$	HCCH-E.COSY
v_4		
χ	$^3J(H1',C2)$; $^3J(H1',C6)$ (in pyrimidines) $^3J(H1',C8)$; $^3J(H1',C4)$ (in purines)	Refocused HMBC

resolution. In a 3D experiment, one has the choice to record either an additional proton (H<u>CCH</u>) or carbon (<u>H</u>CC<u>H</u>) chemical shift dimension. This should be decided based upon the resolution in the proton versus the carbon spectrum. The 2D HCCH-E.COSY of 5'-GMP is shown in Fig. 4. The marked arrows indicate the analysed cross peaks, the H5', H5" resonances are degenerate.

Table 2 lists the vicinal proton–proton coupling constants determined for $^{13}C/^{15}N$-labeled 5'-GMP. The determined coupling constants are in agreement with a C2'-endo/C3'-endo (S/N) ratio of approximately 70%/30%.

The requirement in E.COSY experiments to leave the spin states of the starting proton spin unaffected can be implemented using weighted summation of experiments with different flip angles, 45° and 135°, or alternatively with a single small flip angle (β) pulse. For the experiment with a single $\beta = 36°$ pulse, the ratio of nonconnected to connected transitions equals $\tan^2\beta/2$ (see Fig. 3A). The appearance of nonconnected transitions introduces unsymmetrical signal components which systematically shift the submultiplets together and lead to systematically smaller

TABLE 2
VICINAL PROTON-PROTON COUPLING CONSTANTS OF $^{13}C/^{15}N$-LABELED 5'-GMP

Coupling constant	Experiment		Cross peak
	β-COSY	44,136-E.COSY	
$^3J(H1',H2')$	5.7 ± 0.1	5.4 ± 0.2	C2',H1'
$^3J(H2',H1')$	5.5 ± 0.1	5.7 ± 0.1	C1',H2'
$^3J(H2',H3')$	4.9 ± 0.1	5.2 ± 0.3	C3',H2'
$^3J(H3',H2')$	4.6 ± 0.1	5.1 ± 0.2	C2',H3'
$^3J(H3',H4')$	3.1 ± 0.1	3.3 ± 0.1	C3',H4'
$^3J(H4',H3')$	3.4 ± 0.1	3.4 ± 0.1	C4',H3'
$^3J(H4',H5')$	H5' and H5" are degenerate		

Coupling constants were determined with two different techniques (see text). Experimental conditions: D_2O, pD = 9.

A: 2D–HCCH–E.COSY

^{1}H β β $\beta+90$ β $\Delta/2$ $\Delta/2$ $\Delta/2$ β β x $\Delta'/2$ $\Delta/2$ $\Delta/2$ $t_2^{\phi+\psi}$

^{13}C^{aliphatic} (ϕ) $\tau/2+t_1/2$ $\tau/2-t_1/2$ y $\tau'/2$ (ψ) $\tau'/2$ GARP

^{31}P   GARP

B: 2D P–FIDS–CT–HSQC

^{1}H   x $\Delta/2$ $\Delta/2$ y $\Delta/2$ $\Delta/2$ $t_2^{\phi+\psi}$

^{13}C^{aliphatic} (ϕ) $t_1/2$ $\tau/2$ $\tau/2-t_1/2$ (ψ) GARP

Experiment 1 ^{31}P   x −x   GARP

Experiment 2 ^{31}P   x x

C: refocused HMBC

^{1}H   x Δ Δ $t_2^{\phi+\psi}$

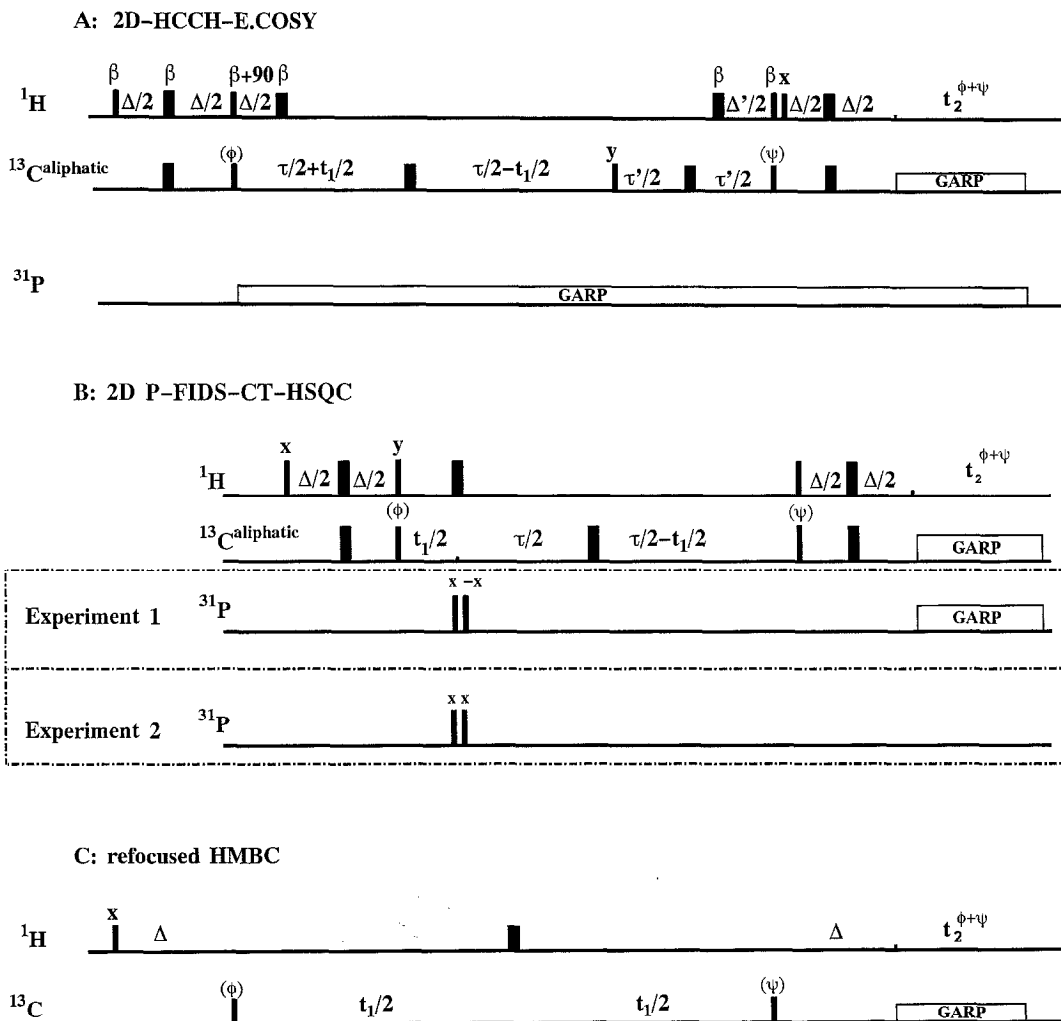^{13}C (ϕ) $t_1/2$ $t_1/2$ (ψ) GARP

Fig. 2. (A) 2D HCCH-E.COSY experiment. Nonselective carbon pulses were used, $\Delta = 3.02$ ms, $\Delta' = 1.648$ ms, $\tau = 3/(4$ ^{1}J(C,C)) = 18.74 ms, $\tau' = 1/(4\ ^1$J(C,C)) = 6.25 ms. In the 44,136-HCCH-E.COSY, four scans with $\beta = 44.4°$ and 24 scans with $\beta = 135.6°$ and inverted receiver phase were recorded. In the HCCH-E.COSY with a single flip angle, instead of phase shifting all preceding 90° and 180° proton pulses, only one β pulse of 36° was used in the second INEPT step (32 scans). 132 experiments in t_1 were recorded. Frequency sign discrimination was achieved with TPPI (Marion and Wüthrich, 1983) on the first carbon pulse. Total measurement times were 3 h for each experiment on a Bruker AMX 400, equipped with a triple resonance ^{1}H,^{13}C broadband 5 mm probe. For the four scans, the phase cycle is: $\phi = $ x,−x; $\psi = $ x,x,−x,−x. (B) CT-P-FIDS-HSQC, with and without ^{31}P decoupling in ω_1 and ω_2. Experiment 1 is recorded with a 90$_x$ and a 90$_{-x}$ ^{31}P pulse, amounting to evolution of the ^{13}C,^{31}P coupling during t_1 and with decoupling of phosphorus during t_2. In experiment 2, the two 90$_x$ ^{31}P pulses lead to decoupling of the ^{13}C,^{31}P coupling during t_1. During t_2, the ^{1}H,^{31}P coupling is retained. The phase cycle is: $\phi = $ x,−x; $\psi = $ x,x,−x,−x. $\Delta = 3.02$ ms, $\tau = 3/J = 75$ ms, 264 complex points in t_1 with eight scans per increment were recorded. Frequency sign discrimination was achieved with States-TPPI (Bax et al., 1991) on the first carbon pulse. Total measurement times were 7 h for both experiments. (C) Refocused ^{1}H,^{13}C-HMBC for the measurement of long-range proton–carbon coupling constants. Δ was chosen to be 41, 58.2, 59 or 60 ms. 128 experiments in t_1 with 16 scans per increment were recorded. The total measurement time was 1.5 h. The phase cycle is: $\phi = $ x,−x; $\psi = $ x,x,−x,−x.

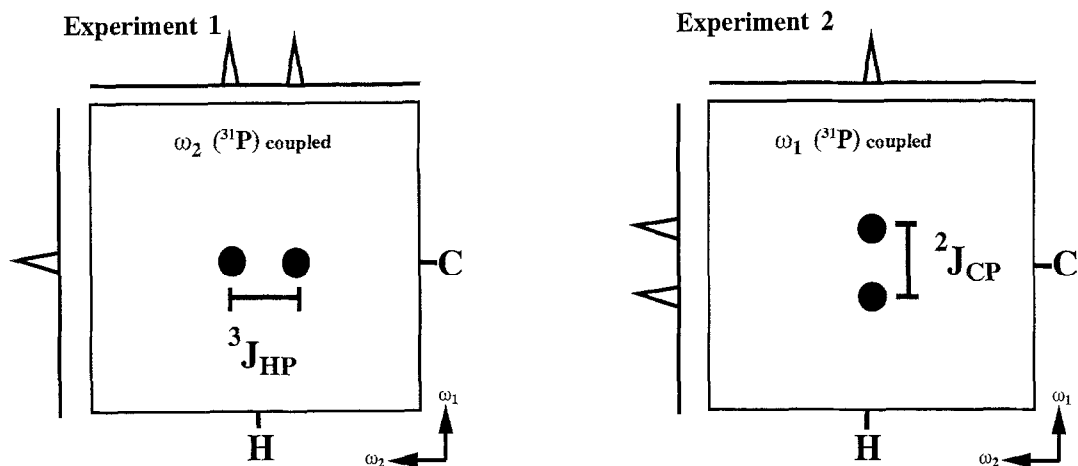## A: HCCH–E.COSY Experiment
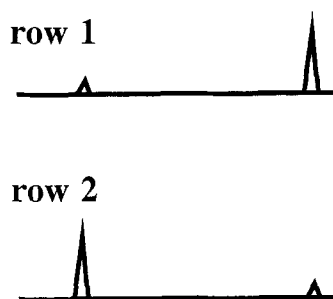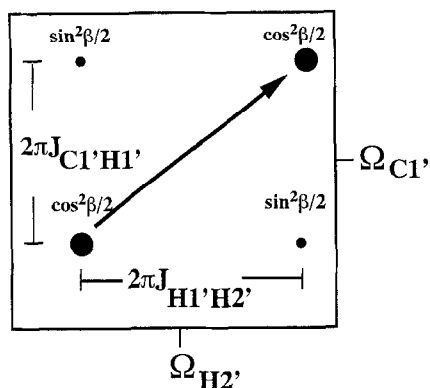
B: P–FIDS–CT–HSQC Experiment

Fig. 3. (A) Schematic multiplet pattern for HCCH-E.COSY with a single flip angle β. The two rows displaced in ω_2 are shown. (B) Schematic multiplet pattern for P-FIDS-HSQC. In experiment 1, J(C,P) is refocused in ω_1; J(H,P) evolves in ω_2. In experiment 2, J(C,P) evolves in ω_1; J(H,P) is refocused in ω_2. Summation along the doublet in ω_2 in experiment 1 yields a singlet in the ω_1 dimension, as indicated in the ω_1 projection. This singlet serves as a reference to fit the J(C,P) coupling evolving in ω_1 in experiment 2.

coupling constants. There are two ways to solve this problem. The first removes the undesired component due to coherence transfer between nonconnected transitions by a post-acquisition processing procedure (method a), the second removes it by recording an experiment with a second flip angle (method b).

(a) For the experiment with a single β angle, multiplying row1 (row2) by $\tan^2\beta/2 = 0.11$ and subtracting the resulting row from row2 (row1) scales the undesired multiplet component to $\tan^4(\beta/2) = 0.01$. This considerably reduces the contributions from the nonconnected transitions.

(b) The undesired nonconnected transitions can be removed by recording an ($\ell = 1$, $N_K = 2$)-
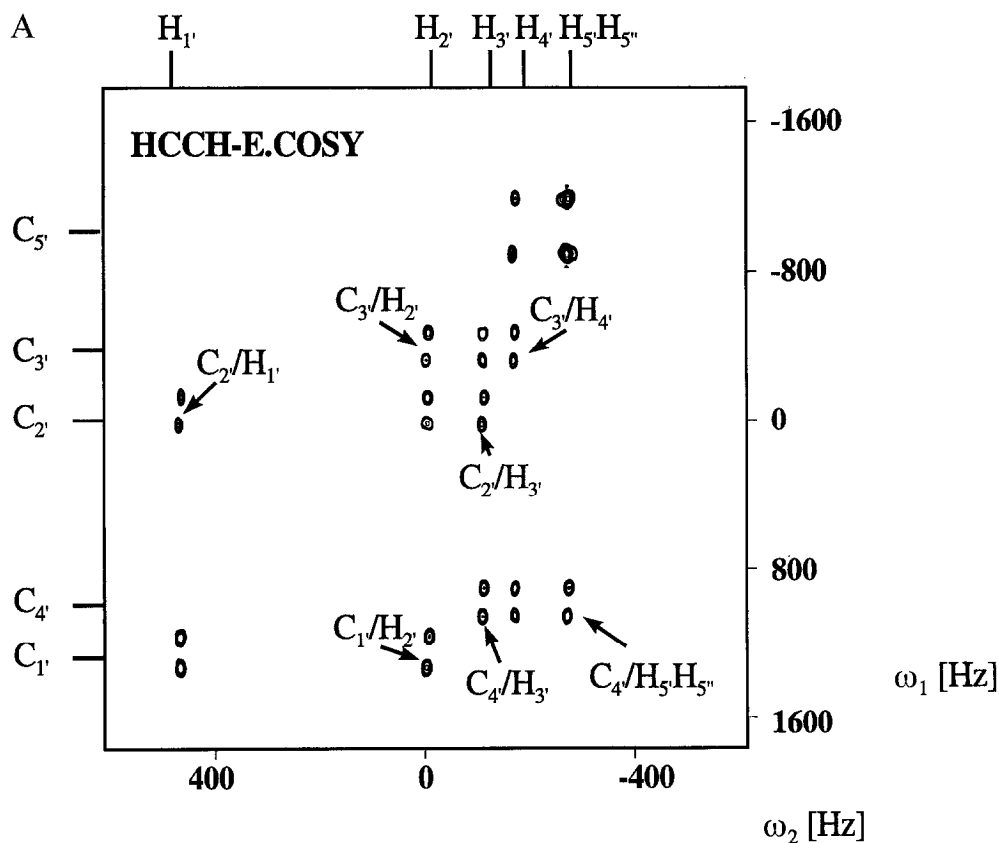
636

Fig. 4. (A) HCCH-E.COSY spectrum with β flip angle for $^{13}C/^{15}N$-labeled 5'-GMP (5.8 mg in 0.5 ml D_2O, 32 mM). The cross peaks that were evaluated are marked with arrows. The doublet structure in the two frequency dimensions ω_1 and ω_2 is clearly visible.

E.COSY (Griesinger et al., 1986) since the spin system used in the HCCH-E.COSY experiment is a two-spin system with one active proton and another proton that remains passive. This requires two experiments with flip angles β = 45° and 135°, with weights 1 and −5.8. In practice, instead of varying the flip angle β, two 90° pulses with a phase shift of β are applied. In order to avoid artifacts from transverse proton magnetization before the C → H transfer, all previous proton pulses are also phase shifted by β. In order to check whether β = 45° and 135° are optimal, a numerical optimization of the amplitude of the desired transfer F (Eq. 1) is performed with the constraint to totally suppress the undesired components (Eq. 2).

$$\frac{\frac{1}{2}(p\,\sin\beta_1\cos^2\beta_1 + \sin\beta_2\cos^2\beta_2)}{1 + |p|} = F \tag{1}$$

$$\tfrac{1}{2}(p\,\sin\beta_1\sin^2\beta_1 + \sin\beta_2\sin^2\beta_2) = 0 \tag{2}$$

where p is the weight for the experiment with β_1. Figure 6 shows graphically the sensitivity
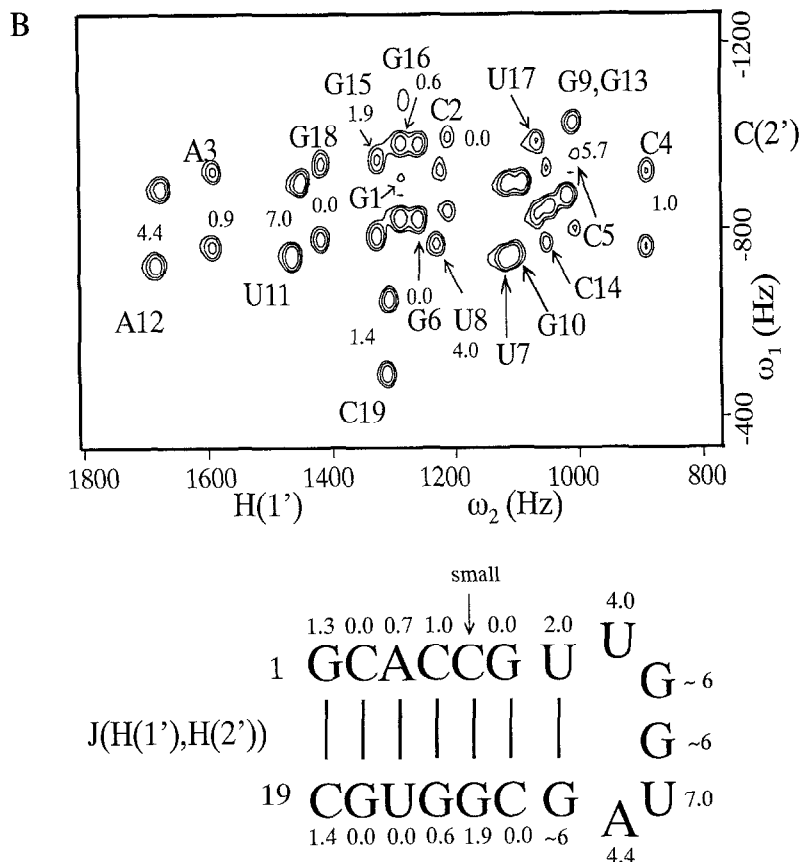
Fig. 4. (B) C2',H1' region of the 2D HCCH-E.COSY experiment of the 19-mer RNA as given in the text. Nonselective carbon pulses were used, $\Delta = 3.02$ ms, $\Delta' = 1.648$ ms, $\tau = 3/(4J(C,C)) = 18.74$ ms, $\tau' = 1/(4J(C,C)) = 6.25$ ms. A β pulse of 45° was used. Compensation of contributions due to nonconnected transitions was achieved by the tan-multiplication procedure (method a) described in the text. Assignments together with the extracted coupling constants are given in the figure. The H1',H2' coupling for C5 is small, but was not exactly determined due to low signal-to-noise ratio. G13 and G10 overlap entirely in this region. Therefore, the coupling constants are only estimated. The H1',H2' coupling constants differ markedly in the stem and in the loop region. The experiment ran for 2 h on a Bruker AMX 600, equipped with a gradient triple ^{1}H,^{13}C, broadband 5 mm probe.

function F depending on the two flip angles used. The optimum (F = 0.5) is indeed found for $\beta_1 = 45°$ and $\beta_2 = 135°$. This compares well with F = 0.53 for the experiment with a single $\beta = 36°$ pulse. The experiment was performed with $\beta = 44.2°$ and 135.8° to obtain the weights 6 and −1.

For both methods that yield spectra without undesired nonconnected transitions, the following procedure (Schwalbe et al. 1993a,b) is applied to extract coupling constants. An ω_1 summation to increase the signal-to-noise ratio yields one-dimensional rows that are displaced in ω_2, due to the ^{3}J(H,H) coupling. After inverse Fourier transformation and zero-filling to increase the digital resolution, row2 (see Fig. 3A) is shifted by an incremented frequency shift with a step size of 0.037 Hz (from −1.0 to 8.0 Hz), and squared after subtracting from row1. The power integral over this difference spectrum (error integral) versus the shift (Hz) is plotted in Fig. 5B for corresponding
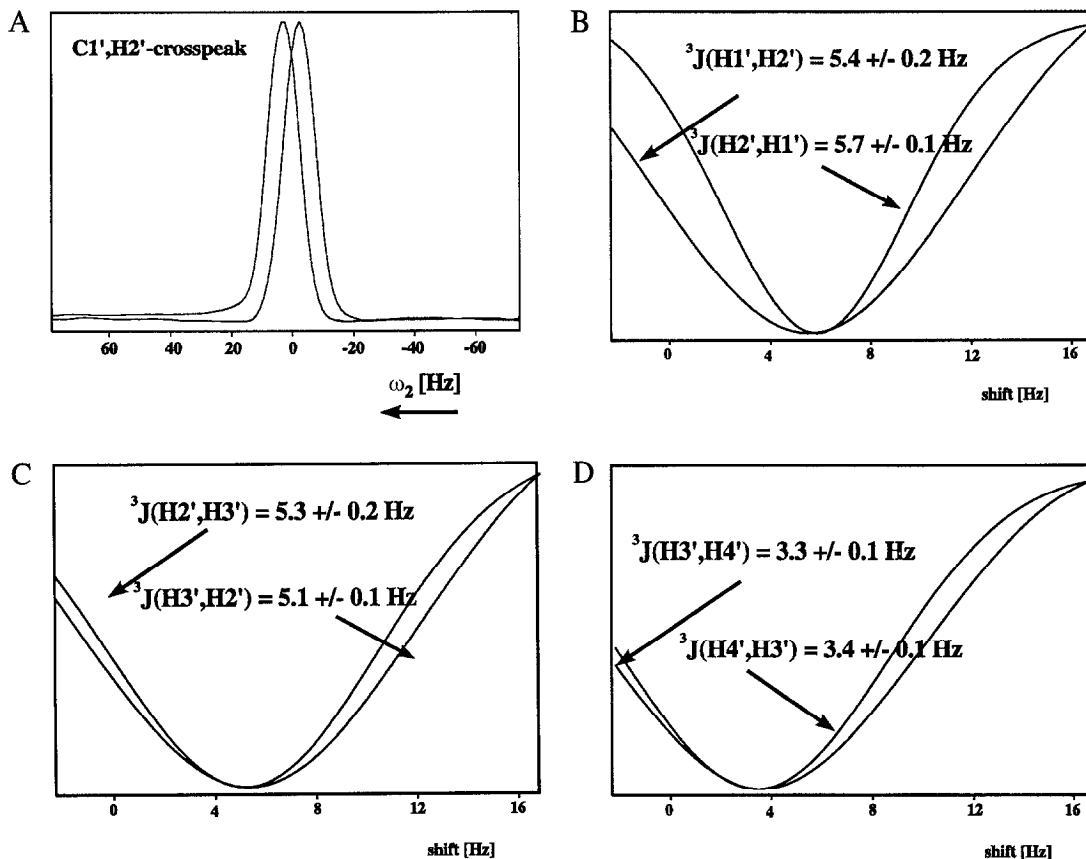
Fig. 5. (A) ω_2 traces through the C1',H2' cross peak of 5'-GMP, showing the slight phase shift introduced by the evolution of the $^3J(H1',H2')$ coupling constant during the last delay Δ. The phase difference can be compensated for during the fitting routine, as described in the text. (B–D) Integral of the power-difference spectrum as a function of the displacement of the two rows, extracted from the 2D HCCH-E.COSY experiment after summation over appropriate traces along ω_1. The rms of the coupling is obtained by variation of the integration region and horizontal extrapolation of the resulting error bar on the minimum.

cross peaks (for example C1',H2' and C2',H1'). The rms deviation of the $^3J(H,H)$ value is determined in the following way. The integration region of the power difference spectrum is varied. The rms of the noise is added to the minimum of the error integral. Varying the integration region over the power difference spectrum provides a noise-dependent measure for the mininum value. The resulting error bar on the value of the minimum is translated into an error in the determined coupling constant by horizontal extrapolation.

As can be seen in Fig. 5A, the two displaced rows do not have the same phase correction. This is due to the evolution of proton–proton coupling in the refocusing period of the last INEPT step. The acquired phase difference between the upper and lower trace $\Delta\phi$ depends on the size of the desired $^3J(H,H)$ coupling and the refocusing delay as given in Eq. 3:

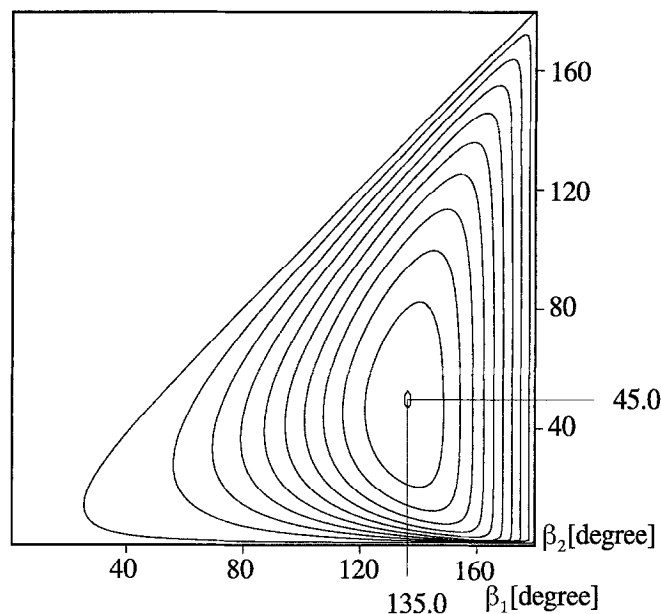$$\Delta\phi = \Delta \, 360° \cdot {}^3J(H,H) \qquad (3)$$

Fig. 6. Two-dimensional plot of the relative sensitivities in weighted HCCH-E.COSY experiments, using two different mixing pulses β_1 and β_2. The optimal flip angles with rational weighting factors 1 and -6 are 44.2 and 135.8, respectively. The intensity of the lowest contour line is 0.05, the contour level increment is 10% of the maximum.

The multiplets are therefore phase corrected according to the shift of the test coupling in Hz as defined in Eq. 3. The whole spectrum is phase corrected before the fitting routine, in order to minimize dispersive components. This phase correction, however, is not a critical condition for the success of the fitting routine.

The HCCH-E.COSY method was applied to a 1.5 mM sample of a uniformly $^{13}C/^{15}N$-labeled 19-mer RNA oligonucleotide: 5'-GCACCGUUGGUAGCGGUGC-3', shown in Fig. 4B. The RNA was prepared by T7 polymerase transcription (Milligan et al., 1987) using $^{13}C/^{15}N$-labeled NTPs (Batey et al., 1992; Nikonowicz et al., 1992). The 19-mer RNA, which forms a stem-loop structure, is derived from RNA I, a repressor molecule in the Col E1 replication control system (Eguchi et al., 1991). Figure 4A shows the C2',H1' region of the HCCH-E.COSY spectrum (measuring time 2 h) of the 19-mer. The spectrum clearly shows the displacement due to the homonuclear coupling constants. $^3J(H1',H2')$ coupling constants are clearly distinct between the loop region and the stem region. The small $^3J(H1',H2')$ coupling constants observed in the stem region are in agreement with an A-RNA structure, whereas the larger $^3J(H1',H2')$ coupling constants in the loop probably indicate conformational equilibria.

$^3J(H,P)$ AND $^3J(C,P)$ COUPLING CONSTANTS

Recently, we have introduced a method to determine vicinal J(H,P) and J(C,P) coupling constants in DNA and RNA samples with carbon in natural abundance (Schwalbe et al., 1993b). The method relies on fitting the desired long-range coupling from a reference multiplet that does not contain the heteronuclear coupling of interest. The coupled multiplet can be obtained by record-

ing a ^{1}H,^{13}C-HSQC experiment with ^{31}P decoupling in ω_1 (experiment 1) or in ω_2 (experiment 2), as shown in Figs. 2B (pulse sequence) and 3B (schematic multiplet pattern). The couplings to ^{31}P evolve as $J(H,P)$ in ω_2 in experiment 1 and as $J(C,P)$ couplings in ω_1 in experiment 2. After summation over the doublet along ω_2 in experiment 1, the obtained singlet serves as the reference singlet for fitting of the $J(C,P)$ in experiment 2. Summation over the multiplet in ω_1 in experiment 2 yields a singlet to fit the $J(H,P)$ coupling in experiment 1.

Application of the P-FIDS method to uniformly ^{13}C-labeled RNA samples requires constant-time evolution in ω_1 to suppress homonuclear carbon–carbon couplings. In the ω_1-^{31}P-decoupled ^{1}H,^{13}C-CT-HSQC experiment (Santoro and King, 1992; Vuister and Bax, 1992) the attainable resolution, which is inversely proportional to the maximum value of the constant-time period, depends upon the transverse relaxation time of carbon single-quantum coherence and the attenuation of the signal due to long-range carbon–carbon couplings. We have chosen $\tau = 3/J$ as constant-time period, yielding a $t_1^{max} = 37.5$ ms. The C4',H4' cross peak of 5'-GMP is shown in Fig. 7.

The vicinal carbon–phosphorus and proton–phosphorus coupling constants determined for ^{13}C,^{15}N-labeled 5'-GMP are as follows: $^3J(C4',P) = 8.6$ Hz, $^2J(C5',P) = 5.2$ Hz and $^4J(H4',P) = 1.1$ Hz. The H5',H5" protons are degenerate. The statistical error of the coupling constants due to noise (Schwalbe et al., 1993a) is below 0.1 Hz. The $^3J(C4',P)$ coupling constant of 8.6 Hz corresponds to an average between the three possible staggered conformations.

The C5',H5'/H5" cross-peak region, together with the derived $^3J(H5',P)$ and $^3J(H5",P)$ coupling constants from some assigned cross peaks, obtained from application of the P-FIDS-CT-HSQC to the 19-mer RNA, are shown in Fig. 7C. There is no large variation of coupling constants in the RNA fragment, indicating little change of backbone torsional angles between stem and loop.

LONG-RANGE PROTON CARBON COUPLINGS FOR THE DETERMINATION OF THE SYN VERSUS ANTI CONFORMATION AROUND χ

$^3J(H1',C)$ couplings to the C8,C4 carbons in purine nucleotides and to the C2,C6 carbons in pyrimidine nucleotides depend on the torsion angle χ. They can be used to determine the syn/anti conformation around the glycosidic bond (Lamieux et al., 1978). In refocused HMBC spectra (Bermel et al., 1989; Bax et al., 1992; Vuister et al., 1993; Zhu and Bax, 1993) (Fig. 2C), the relative intensities of various cross peaks can be used to determine the size of long-range coupling constants. One could also use this experiment for another structurally interesting question, i.e., the stereochemical assignment of the two diastereotopic H5',H5" protons in RNA and DNA, by the measurement of $^3J(C3',H5')$ and $^3J(C3',H5")$ coupling constants. In contrast to the H2',H2" protons in DNA, the H5',H5" protons cannot readily be assigned based on chemical shift arguments.

If the dependence of the *relative* transfer amplitude on the active coupling constant is known in the refocused HMBC, one can deduce the size of an interesting coupling by comparing its cross-peak intensity with the intensity of a cross peak with known coupling constant. Thus, the intensity of the C8,H1' cross peak, for example, is proportional to:

$$I_{C8,H1'} \sim k * \sin^2(\pi \ ^3J(H1',C8) \ \Delta) * \cos^2(\pi \ ^1J(H1',C1') \ \Delta) \tag{4}$$

whereas the cross-peak intensity of the C1',H1' cross peak is proportional to:

A

C4',H4'-crosspeak

ω_1 ^{31}P-coupled

ω_1 ^{31}P-decoupled

80   40   0   -40   -80

ω_1 [Hz]

B

^{3}J(C4',P)=8.6 Hz

simulated multiplet

experimental multiplet

difference

30   10   -10   -30

ω_1 [Hz]

C

A12

G13

6.3   U11   5.2

8.6   5.7   G9/G10

C19

G1   9.4   C2   5.1

9.4   U8   5.8

10.8   G15   5.1

G18   G16

A3   A3

7.4   5.3   G18   C5

C5

G6,C4   G6,C4

U7,U17,C14   U7,U17,C14

-100   -200   -300   -400

H(5',5") ω_2 (Hz)

C(5')

ω_1 (Hz)

2600   2400   2200   2000

9.4; 7.4;
5.1 5.3

1 GCACCG U U $^{9.4;5.8}$

J(H5^d,P);

J(H5^u,P)

G

G

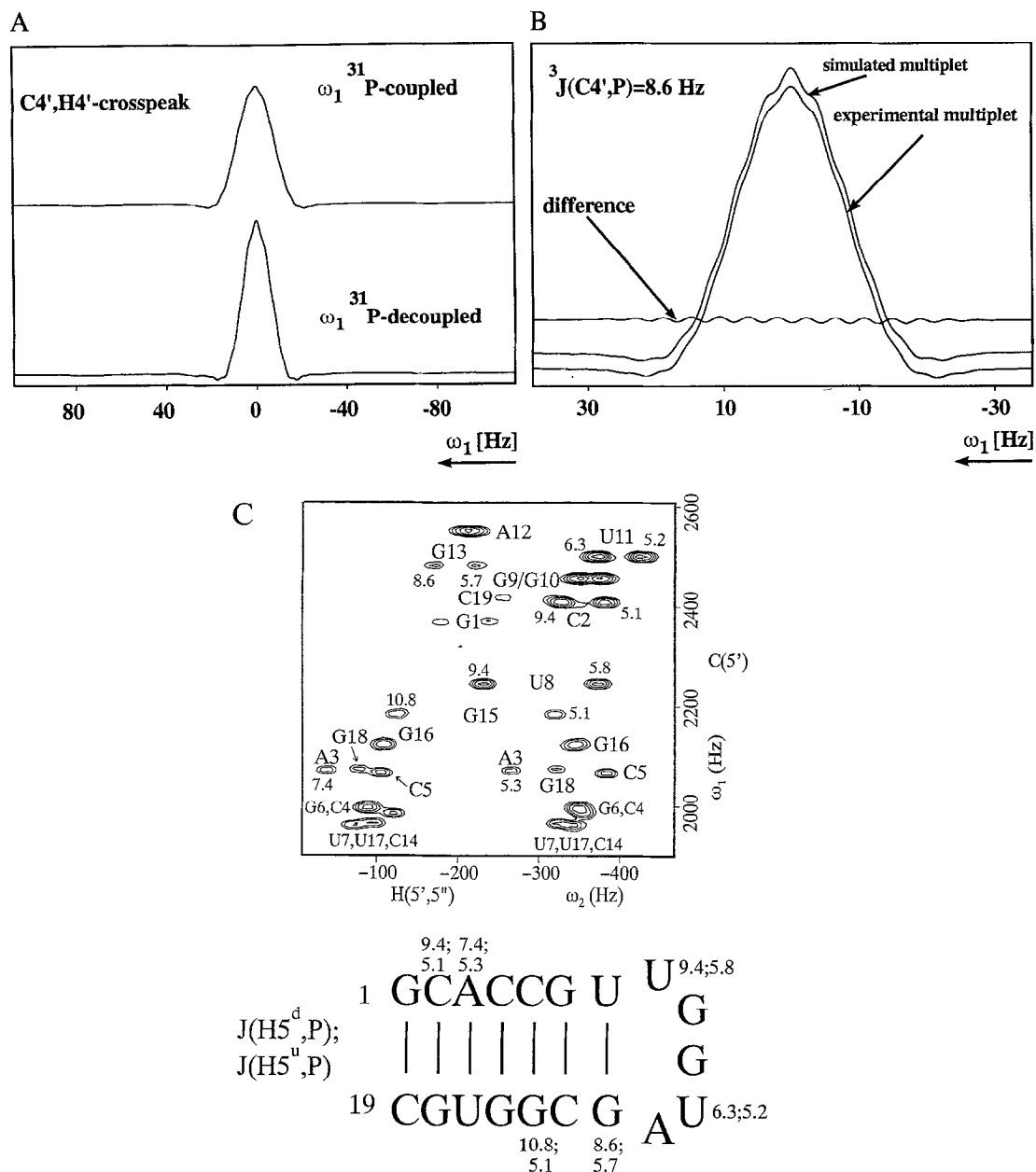19 CGUGGC G A U $^{6.3;5.2}$

10.8;   8.6;
5.1   5.7

Fig. 7. (A) ω_1 trace through the C4',H4' cross peak in a CT-P-FIDS-HSQC. The top trace shows the C4' resonance without, and the bottom trace with phosphorus decoupling. (B) Convolution of the bottom multiplet from (A) with an in-phase trial coupling yields the 'simulated' multiplet. The fit to the coupled multiplet is optimal for ^{3}J(C4',P) = 8.6 Hz. The difference between the simulated and experimental multiplet is rather small. (C) H5',5",C5' region of the CT-P-FIDS-HSQC of the 19-mer RNA (see bottom of the figure). Four scans were used; the constant-time delay is: τ = 3/J(C,C) = 75 ms, t_1^{max} = τ/2. Some assignments, together with ^{3}J(H5',P) and ^{3}J(H5",P) coupling constants are given. The coupling constants for A12 and U7 could not be determined due to strong coupling of the H5' and H5" protons. The ω_1 axis is upside down, due to folding. The coupling constants in the stem region are in agreement with values found earlier for canonical A-RNA (Davis et al., 1993).

TABLE 3

CROSS-PEAK INTENSITIES IN THE ω_2-^{13}C-COUPLED HSQC AND RESULTING COUPLING CONSTANTS AS A FUNCTION OF MAGNETIZATION TRANSFER DELAY

Magnetization transfer delay Δ (ms)	Experimental intensities of cross peaks			Coupling constant		
	C1',H1'	C4,H1'	C8,H1'	C1',H1'	C4,H1'[a]	C8,H1'[b]
41	45.5	10.2	34.3	165.9	2.5	4.3
58.2	335.4	51.2	113.8	165.9	3.5	4.5
59	170.8	73.8	287.8	165.9	2.6	4.3
60	7.5	101.9	432.1	165.9	2.6	4.4

[a] Experimental $^3J(C4,H1') = 2.8 \pm 0.4$ Hz.
[b] Experimental $^3J(C8,H1') = 4.4 \pm 0.1$ Hz.

$$I_{C1',H1'} \sim k*\sin^2(\pi\ ^1J(H1',C1')\ \Delta)*\cos^2(\pi\ ^3J(H1',C8)\ \Delta) \tag{5}$$

with k summarising all passive couplings. The passive couplings contribute to the same extent to both cross peaks if one measures cross peaks to the same proton in t_2, and can be neglected in the following. The ratio of cross-peak intensities is therefore:

$$\frac{I_{C8,H1'}}{I_{C1',H1'}} = \frac{\tan^2(\pi\ ^3J(H1',C8)\ \Delta)}{\tan^2(\pi\ ^1J(H1',C1')\ \Delta)} \tag{6}$$

Knowing the $^1J(H1',C1')$ coupling, for example from an ω_2-^{13}C-coupled HSQC, the desired coupling constant $^3J(H1',H8)$ is given by:

$$^3J(H1',C8) = (\pi\Delta)^{-1}\arctan\ [(I_{H1',C8}/I_{C1,H1'})^{1/2}\ \tan\ \pi\ ^1J(H1',C1')\Delta] \tag{7}$$

Table 3 lists the cross-peak intensities and the resulting coupling constants for various magnetization transfer delays Δ. The coupling constants determined are in agreement with a conformational equilibrium between syn and anti, with a slight predominance of the anti conformation ($^3J(C8,H1') > ^3J(C4,H1')$).

CONCLUSIONS

We have introduced three experiments that can be used to measure conformationally relevant homo- and heteronuclear coupling constants in uniformly ^{13}C-labeled RNA oligomers. These experiments will also be applicable to DNA oligomers when ^{13}C-labeled DNA becomes available. In the HCCH-E.COSY experiment, proton–proton couplings may be measured. The method can be applied to macromolecules. The experiment has high sensitivity, since magnetization transfer processes rely on large $^1J(H,C)$ and $^1J(C,C)$ couplings only. It uses nonselective carbon pulses, making implementation straightforward. We expect that application of this technique will provide direct insight into the conformation of individual ribosyl units. Some experimental drawbacks have been remedied. It has been shown that systematic errors in the determination of proton–proton coupling constants, due to phase distortions stemming from the evolution of

homonuclear coupling in the second refocusing period of the HSQC sequence, amount to approximately 10% of the size of the coupling constant and can be compensated for by appropriate extraction procedures. Another source of systematic errors in the determination of the homonuclear coupling constants has recently been pointed out (Harbison, 1993; Norwood, 1993). Differential relaxation for in-phase and antiphase proton magnetization leads to systematically smaller couplings in E.COSY-based experiments. Since the relaxation of proton magnetization in RNA oligomers is mainly governed by the dipole–dipole interaction between vicinal and (for the H5',H5" protons) geminal protons, the systematic errors introduced depend on the sugar conformation and on the local correlation times, which in turn depend on the molecular weight.

In the P-FIDS-CT-HSQC-experiment, $^{n}J(C,P)$ and $^{n}J(H,P)$ couplings can be determined in order to examine the phosphodiester backbone conformation. The sensitivity of this experiment is the same as in the usual $^{1}H,^{13}C$-CT-HSQC. A detailed analysis of the precision as well as the accuracy of the method, depending on the signal-to-noise ratio of the experiments and the linewidth of the sample, has been discussed by Schwalbe et al. (1993a).

Measuring the long-range proton–carbon couplings from H1' to C8 and C4 in purines and from H1' to C2 and C6 in pyrimidines yields NOE-independent information of the syn/anti equilibrium around the angle χ, facilitating an exact conformational analysis. This experiment can also be used to derive the stereospecific assignment of the H5',H5" protons in oligonucleotides.

ACKNOWLEDGEMENTS

REFERENCES

Batey, R.T., Inada, M., Kujawinski, E., Puglisi, J.D. and Williamson, J.R. (1992) *Nucleic Acids Res.*, **20**, 4515–4523.
Bax, A., Ikura, M., Kay, L.E. and Zhu, G. (1991) *J. Magn. Reson.*, **91**, 174–178.
Bax, A., Max, D. and Zax, D. (1992) *J. Am. Chem. Soc.*, **114**, 6924–6925.
Bermel, W., Wagner, K. and Griesinger, C. (1989) *J. Magn. Reson.*, **83**, 223–232.
Davis, P.W., Thurmes, W. and Tinoco Jr., I. (1993) *Nucleic Acids Res.*, **21**, 537–545.
Eggenberger, U., Karimi-Nejad, Y., Thüring, H., Rüterjans, H. and Griesinger, C. (1992) *J. Biomol. NMR*, **2**, 583–590.
Eguchi, Y., Itoh, T. and Tomizaw, J. (1991) *Annu. Rev. Biochem.*, **60**, 631–652.
Griesinger, C., Sørensen, O.W. and Ernst, R.R. (1985) *J. Am. Chem. Soc.*, **107**, 6394–6396.
Griesinger, C., Sørensen, O.W. and Ernst, R.R. (1986) *J. Chem. Phys.*, **85**, 6837–6852.
Griesinger, C., Sørensen, O.W. and Ernst, R.R. (1987) *J. Magn. Reson.*, **75**, 474–492.
Griesinger, C. and Eggenberger, U. (1992) *J. Magn. Reson.*, **97**, 426–434.
Harbison, G.S. (1993) *J. Am. Chem. Soc.*, **115**, 3026–3027.
Lamieux, R.U., Nagabushan, L. and Paul, B. (1978) *Can. J. Chem.*, **50**, 773–776.
Marion, D. and Wüthrich, K. (1983) *Biochem. Biophys. Res. Commun.*, **113**, 967–974.
Marion, D. and Bax, A. (1988) *J. Magn. Reson.*, **80**, 528–533.
Michnicka, M.J., Harper, J.W. and King, G.C. (1993) *Biochemistry*, **32**, 395–400.
Milligan, J.F., Groebe, D.R., Witherell, G.W. and Uhlenbeck, O.C. (1987) *Nucleic Acids Res.*, **15**, 8783–8798.

Müller, L. (1987) *J. Magn. Reson.*, **97**, 191–194.

Nikonowicz, E.P. and Pardi, A. (1992) *Nature*, **335**, 184–186.

Nikowicz, E.P., Sirr, A., Legault, P., Jucker, F.M., Baer, L.M. and Pardi, A. (1992) *Nucleic Acids Res.*, **20**, 4507–4513.

Norwood, T.J. (1993) *J. Magn. Reson.*, **101**, 109–112.

Sänger, W. (1988) *Principles of Nucleic Acid Structure*, 2nd ed., Springer, New York, NY.

Santoro, J. and King, G.C. (1992) *J. Magn. Reson.*, **97**, 202–207.

Schwalbc, H., Samstag, W., Engels, J.W., Bermel, W. and Griesinger, C. (1993a) *J. Biomol. NMR*, **3**, 479–486.

Schwalbe, H., Rexroth, A., Eggenberger, U., Geppert, T. and Griesinger, C. (1993b) *J. Am. Chem. Soc.*, **115**, 7878–7879

Van Wijk, J., Huckriede, B.D., Ippel, J.H. and Altona, C. (1992) *Methods Enzymol.*, **211**, 286–306.

Varani, G. and Tinoco Jr., I. (1991) *Q. Rev. Biophys.*, **4**, 479–532.

Vuister, G.W. and Bax, A. (1992) *J. Magn. Reson.*, **98**, 428–435.

Vuister, G.W., Wang, A.C. and Bax, A. (1993) *J. Am. Chem. Soc.*, **115**, 5334–5335.

Zhu, G. and Bax, A. (1993) *J. Magn. Reson.*, **104**, 353–357.